First thermal fatigue studies of tungsten armor for DEMO and ITER at the OLMAT High Heat Flux facility

D. Alegre [a,*], D. Tafalla [a], A. De Castro [a], M. González [a], J.G. Manchón [a], F.L. Tabarés [a], T. Hernández [a], M. Wirtz [b], J.W. Coenen [b,c], Y. Mao [b], E. Oyarzábal [a], the OLMAT team

[a] Laboratorio Nacional de Fusión. CIEMAT, Av Complutense 40, 28040 Madrid, Spain
[b] Forschungszentrum Jülich GmbH, Institut für Energie- und Klimaforschung - Plasmaphysik, 52425 Jülich, Germany
[c] Department of Nuclear Engineering & Engineering Physics, University of Wisconsin Madison, Madison, WI 53706, USA

ARTICLE INFO

ABSTRACT

The armor for future nuclear fusion reactors is one of the main areas of research due to the harsh conditions it will undergo. Thermal fatigue is one of the most serious damage, as it will cause any material to fail even if the heat and particle loads during the reactor operation are always maintained low. In this work we have compared the actual tungsten armor for ITER tokamak with a new advanced tungsten material: tungsten reinforced by tungsten fibers (Wf/W). ITER-like W has shown small intergranular cracking at heat loads similar to the ones found in other similar devices: heat flux factor of $F_{HF} = 5.2 \pm 1.6$ MW/m^{2}s$^{0.5}$. But at much lower number of pulses: 641 versus 10^5. H embrittlement by the high-energy ions of OLMAT has been postulated as one of the main reason of this relatively prompt cracking appearance. Opposed to this, the type of Wf/W studied here, Porous Matrix (PM-Wf/W), has shown no damage at the same conditions and up to 950 pulses. These results show the capabilities of OLMAT for fatigue studies in conditions relevant to a future nuclear fusion reactor. New upgrades of OLMAT will partially solve the issues found in this first phase. Future work to continue with fatigue studies will be addressed.

1. Introduction

Materials resilience is one the main causes of the delay in the achievement of an economically viable nuclear fusion reactor based on magnetic confinement. This is especially true for the inner shielding at the divertor area against the plasma exhaust (i.e. strike points): the target plates [1–6]. Peak steady state power densities up to 20 MW/m^2 may arise during normal operation. Moreover, off-normal transient events like ELMs (Edge Localized Modes), disruptions and VDEs (Vertical Displacement Events), if not mitigated, may lead to fast (few ms) power loads ranging from hundreds MW/m^2 (ELMs) to tens GW/m^2 (disruptions and VDEs) [1–9]. When the critical damage caused by intense neutron bombardment is also considered, the resilience of traditional shielding based on pure tungsten is seriously compromised [4].

For ITER (International Thermonuclear Experimental Reactor) divertor the armor consists on tungsten monoblocks over a CuCrZr heat sink [1]. The microstructure of this tungsten is very specific: perpendicular-to-surface, elongated grains parallel to the heat transfer direction. In this way, the crack propagation, usually intergranular in tungsten [1,4,9–11], is aligned with the grain orientation, so delamination by cracks parallel to the surface is minimized. However, for many reasons, mainly related to the expected huge neutron loads, this material will likely not be apt for DEMO (DEMOnstration reactor) [3,5–9]. Even considering that the replacement of divertor armor in DEMO is scheduled every 1.5 years, when in ITER will be 10 years [1,3,7]. Because of this, many advanced W materials and alloys are being developed to solve the issues already found for pure W: K-doping for higher recrystallization temperature [12,13]; W-Cr-Y alloys to avoid reaction with air in case of accident [14,15]; microstructured W for thermal shock resilience and neutron damage [16]; and, the one tested in this work, W reinforced with W fibers (Wf/W), for its better mechanical properties and resilience against fatigue thanks to its pseudo-ductility [17–19]. However, the improvement in some properties may cause the worsening of others: for example small loses in some mechanical properties of K-doped and W-Cr-Y alloys, poorer thermal conductivity in Wf/W (66 % of pure W [18]),

etc. Therefore, a compromise must be found for each option.

In DEMO and ITER thermal fatigue of the first wall armor will be a main issue [3,5–8]. This fatigue consists on the accumulation of defects like dislocations during the thermal load, leading to crack formation. As they are being heated the materials are subjected to thermal expansion, which is restricted by the colder surrounding material, generating compressive stresses. This process is more critical at the junction of W armor and heat sink (CuCrZr) due to the large thermal expansion mismatch (not within the scope of this work, although it will be studied in the future). Moreover, this defect accumulation, and cracking initiation, will be faster for shorter thermal loads (as ELMs, few ms), larger heat loads, and mainly, when the material is brittle, as the heated part becomes ductile but surrounded by cold, brittle material [10]. In DEMO fatigue cracking is even more dangerous. Brittle cracking will be critical as the Ductile-to-Brittle Transition Temperature (DBTT) of W is expected to increase from 100 to 400 °C (depends critically on fabrication technique and treatments) to around 800 °C because of neutron bombardment [4]. Furthermore, in DEMO many operation conditions: duty factor (time in operation), number of pulses, number of mitigated ELMs, and neutron loading (leading to embrittlement) will be much demanding than in ITER. For example, for mitigated ELMs (2 ms duration) even at heat load as low as 10 MW/m^2, a frequency of tens Hz will be required to achieve this low heat flux. Then 10^6 heat load cycles may be reached in just 10–30 h operation. At that huge number of cycles almost any material tested so far has started to fail [10,11]. This would lead to the operation only in ELM-free modes like QH-mode, I-mode, negative triangularity, etc. But those require large changes in DEMO design (which is too advanced to be easily changed) and/or worse confinement than the usual ELMy H-mode, see [1] and references therein. Therefore, the pragmatic solution is to operate with a reliable mitigated ELMy H-mode, and to design a material much more resilient to thermal fatigue, being the one studied in this work Wf/W the most promising [17–19]. Cracking will appear in neutron-loaded Wf/W as any other W alloy, but thanks to its pseudo-ductility induced by the fibers (extrinsic toughening) the cracks will grow much slower and critical failure may be sufficiently delayed.

In this work we present the first thermal fatigue studies of ITER and DEMO relevant materials in the OLMAT High Heat Flux (HHF) device [20,21]. OLMAT capabilities for thermal fatigue testing will be described in section 2. Fatigue experiment of ITER-like W and W reinforced with W fibers in a Porous Matrix (PM-Wf/W, see [17,18] for details) will be shown in Section 3, and they will be compared to previous results in other HHF devices showing similar results. Finally, in section 4 the conclusions will be given and the future work to continue these studies will be outlined.

2. Material and methods: OLMAT

The OLMAT HHF device has already been described in full [20], as well as its commissioning and first results [21–23]. OLMAT HHF device is still evolving, and this work will be focused on performing fatigue studies of materials relevant to a future nuclear fusion reactor. Only a brief description will be given here, and its schematic can be found in Fig. 1. The OLMAT project uses the TJ-II Counter-NBI injector to irradiate different targets, solid or liquid–metal based ones. Its pumping is independent of TJ-II by means of two turbopumps in series with a rough pump. Pressures of 5·10^{-7} mbar are routinely achieved. As can be seen in Fig. 1 OLMAT is equipped with a large set of diagnostics: 2 infrared (IR) pyrometers of different ranges (OPTRIS CTlaser and OPTRIS 3MH1), calibrated at the laboratory by comparison with E-type thermocouples at the surface; one IR camera (Optris PI 160); 2 E-type thermocouples at the back of the samples; Optical Emission Spectroscopy (OES) by a CMOS-based spectrometer (compact fiber optic covering the 236–812 nm range); a SRS-200 Residual Gas Analyzer; and a compact, fast-camera (AOS PROMON U750 mono) to monitor the sample damage or particles emission.

NBI beam has a power of up to 705 kW, with a particle energy of 3–40 keV and hydrogen flux up to 1.7·10^{22} 1/m^{2}s. It allows power densities of up to 58 ± 14 MW/m^2 in 100 ms pulses and 150 s repetition rate or up to 24 ± 6 MW/m^2 in 150 ms pulses and 30 s repetition rate [21]. The beam presents a Gaussian profile of 11.7 cm of FWHM, and a relatively flat shape at the powers used here < 20 MW/m^2 [24] to assure a homogeneous power density at the samples. The sample holder is shown in Fig. 2. It consists on a TZM alloy (99 % Mo with 0.5 % Ti and
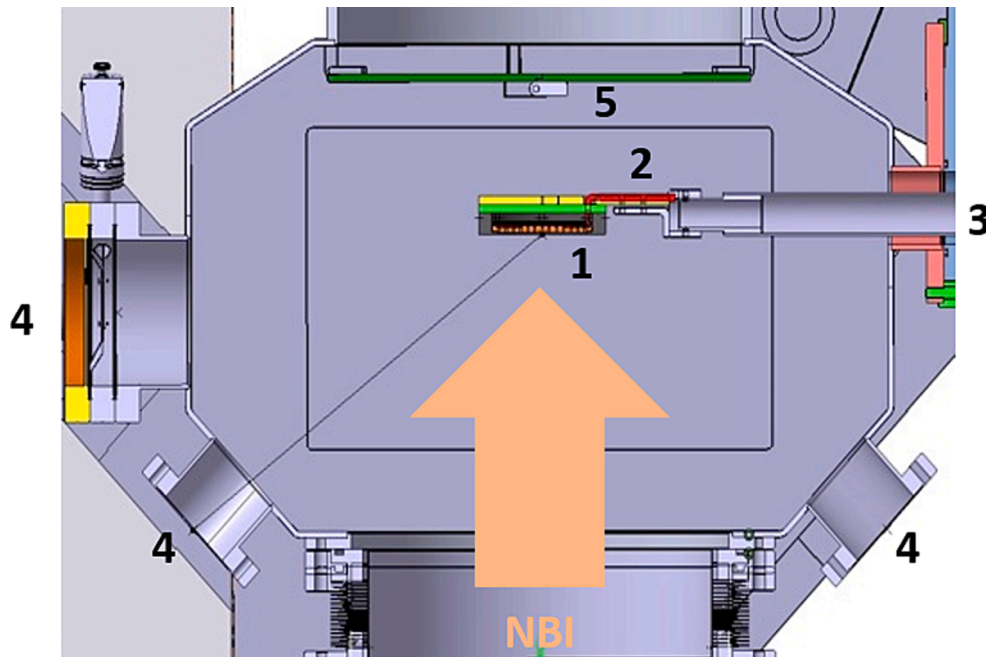
Fig. 1. Top view sketch of the OLMAT experiment with NBI beam depiction. 1. Target with TZM mask and three samples; 2. sample holder in manipulator with rotation/translation capabilities; 3. pre-chamber with RGA; 4. Optical viewports for diagnostics: OES, pyrometers, IR camera and compact fast camera; 5. inertially-cooled, TZM beam dump.
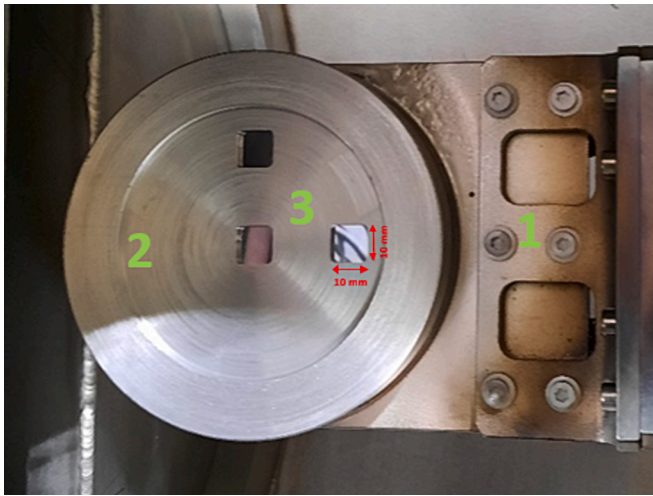
Fig. 2. Stainless steel sample holder (1) with TZM mask (2) and samples (3) with a 10 × 10 mm area exposed.

0.1 % Zr) mask fixed with a TZM cap to a stainless steel sample holder, where 3 samples are fixed: ITER-like W or Porous Matrix PM-Wf/W provided by Jülich FZ from Plansee and fabricated by themselves [17,18] respectively. The three samples are exposed at a slightly different heat flux each one compared to the mean power density: center: +10 %; right −10 %; down mean power. The samples temperature is controlled by a heater placed between the samples and the sample holder. However, as the beam dump is inertially cooled only about 100 consecutive pulses can be done until the system is allowed to cool down to protect the valves, resulting in about 300–400 pulses per day. This will be solved in the future with a water-cooled, large sample holder acting also as beam dump. In order to be able to compare to experiments in other devices like JUDITH2 [11], performed at 700 °C, and to work in the W ductile regime as expected in ITER (T > DBTT, about 250–400 °C [4]) the samples are heated up to a temperature of 425 °C prior the experiment (maximum achievable by the heater), reaching a plateau of ~ 700 °C at surface (by pirometry) in around 15–20 pulses, depending on power. However, in Porous Matrix PM-Wf/W experiments the heater broke and the sample cooled down to 150–200 °C during the technical stop, reaching the ~ 700 °C at surface again in around 20 pulses (relatively fast due to its lower heat conductance and hence slower cooling).

Finally, prior and after the exposure at OLMAT, the erosion of the samples were measured with a W120 balance from Adam Equipment. In the same way, the samples were observed with a Zeiss Auriga Compact FESEM-FIB or by a Leica DCM8 confocal microscope to look for cracking development at surface and cross-section.

3. Results and discussion

During all experiments different diagnostics were monitored. The results for some of them are summarized here:

- *RGA:* a mix of impurities of water and hydrocarbons (m/q ratio range of 14–18 and 26–40) are routinely detected during the NBI pulses. But they are about 2–3 orders of magnitude lower than the hydrogen signal. This indicates that they are the typical impurities at the walls of a long operating device as TJ-II stellarator (which OLMAT is joined with) dragged out by the large surge of pressure from the NBI.
- *OES:* showed a small plasma with a small W emission which develops in front of the surface which is being studied in other works of this group [22,23]
- *IR camera:* showed no difference in samples emission at the end of the series of pulses. Understandable as there is no large cracking.

- *Fast camera:* no particle emission was observed.

Now the results for each material are commented in detail.

3.1. ITER-like W

During almost all pulses the samples temperature were well above the DBTT > 250–400 °C [4]. Around 600–700 °C measured by thermocouples at the back and by pirometry at the surface. This temperature will only allow ductile cracking to occur as will be confirmed later. The samples were exposed to three different OLMAT set of pulses, Table 1:

Being F_{HF} the heat flux factor, which is obtained multiplying the heat flux by the square root of the pulse duration. It has been demonstrated previously that this F_{HF} is HHF device independent (as long as pulse energy distribution has a rectangular shape, and it is not in the ns range or lower), and it is widely used to compare between different HHF devices [10]. In the past, for this ITER-like samples the damage threshold in terms of heat flux at JUDITH2 HHF device was found to be between $F_{HF} = 3$–6 MW/m^{2}s$^{0.5}$ [11]. OLMAT experiments seems to indicate this threshold to be closer to $F_{HF} = 6$ MW/m^{2}s$^{0.5}$ as we have only found damage at 641 pulses of $F_{HF} = 5.2 \pm 1.6$ MW/m^{2}s$^{0.5}$ (sample at the center), with a negligible erosion of < 0.3 mg by gravimetry (within balance error). Surface modification and a small, disperse cracking can be seen in Fig. 3a. This cracking is clearly intergranular as can be observed in SEM cross-section in Fig. 3b. There are some initiated cracks, and only a few of them of 20–30 μm depth, likely the ones observed in upper view SEM. This cracking indicates that our $F_{HF} = 5.2 \pm 1.6$ MW/m^{2}s$^{0.5}$ is close to the damage threshold, as lower values showed no damage, and confirms that OLMAT is able to perform satisfactory fatigue studies. In JUDITH2 10^5 pulses at $F_{HF} = 6$ MW/m^{2}s$^{0.5}$ were needed to observe a small cracking, although some damage was observed since 10^3 pulses [11], while at OLMAT cracking was observed at only 641 pulses. This mismatch may be caused by the different heat loading technique. At OLMAT hydrogen ions in the range of tens keV energy bombard the surface to simulate the heat loads, while in JUDITH2 the energy loads are produced by electron bombardment. So, this difference in pulse number for the cracking threshold may be caused by hydrogen embrittlement on OLMAT due to those high-energy hydrogen ions, as has been found in other works with laser irradiation simulating ELMS combined with continuous plasma in PSI-2 device [25]. In the future, this will be disentangled in OLMAT irradiating at the same power density and number of pulses with the new 90 J CW laser. As it is a pure heat load the thermal fatigue can be separated from the H embrittlement. However, in future fusion nuclear reactors mitigated ELMs will cause hydrogen bombardment in this range of energy [1], so

Table 1
Exposure parameters at OLMAT of ITER-like W and Porous Matrix PM-Wf/W.

material	Pulses	Duration (ms)	Mean heat flux (MW/m^2)	Pulse rate (s)	F_{HF} (MW/m^{2}s$^{0.5}$)
ITER-like W	822	100	8 ± 3	40	2.2 ± 0.8
					2.5 ± 0.9
					2.8 ± 1
	337	150	8 ± 3	40	2.8 ± 1
					3.1 ± 1.1
					3.4 ± 1.2
	641	100	15 ± 5	40	4.2 ± 1.4
					4.7 ± 1.5
					5.2 ± 1.6
PM-Wf/W	934	100	15 ± 5	45	4.2 ± 1.4
					4.7 ± 1.5
					5.2 ± 1.6
	950	100	15 ± 5	45	4.2 ± 1.4
					4.7 ± 1.5
					5.2 ± 1.6
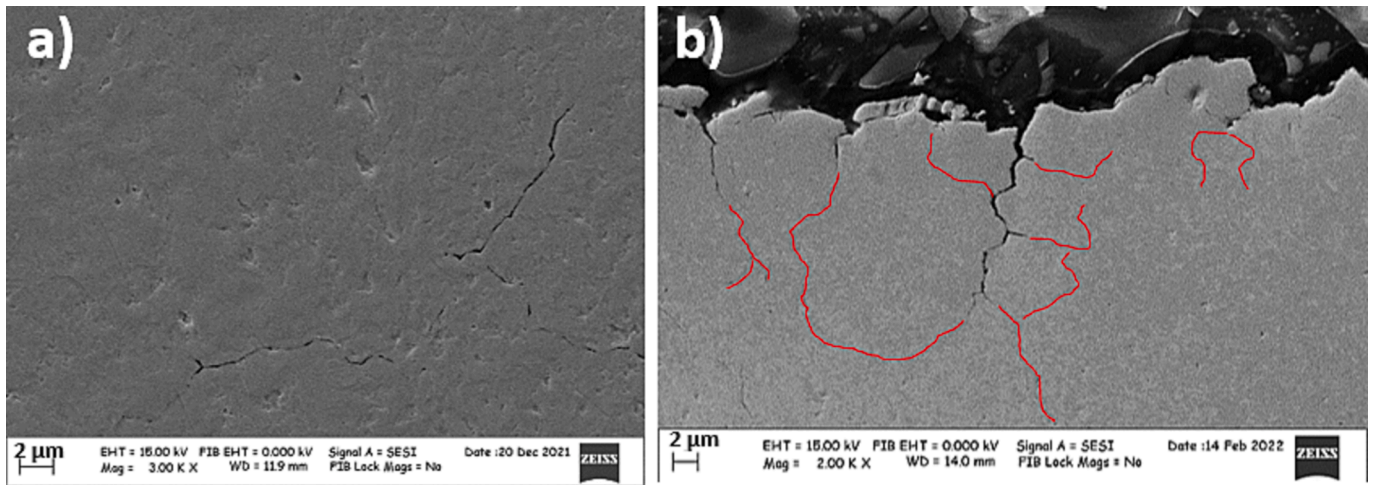
Fig. 3. SEM image of ITER-like sample exposed to 641 pulses of $F_{HF} = 5.2 \pm 1.6$ MW/m²s$^{0.5}$. Small and disperse cracking may be seen in upper view images (a). At cross-section view (b) severe small cracks may be observed initiated between grains, and other larger ones of 20–30 μm depth, clearly intergranular. Red lines have been drawn to help to identify the grain borders, but are only intended as a guide the eye. (For interpretation of the references to colour in this figure legend, the reader is referred to the web version of this article.)

this reduced damage threshold found here may be relevant. On the other hand, in a future nuclear fusion reactor the first wall armor will likely not be polished, opposed to the polished samples used here and in most works. The reasons for this are merely economic, but also to an observed decrease in erosion by sputtering in rough samples [17]. However, a balance should be found, as polishing induces compressive residual stress at the surface, which are good at hinder crack formation and crack growth [26].

As previously mentioned, in this set of samples only ductile fatigue cracking should occur. The repeatedly applied loads and the accumulation of defects like dislocations will cause the initiation of small cracks after a large number of loads. Once formed, these cracks will constantly grow under further loading deeper into the material [11]. Here, as in Fig. 3b, some small, initiated cracks have been detected. But due to the limited number of pulses available in OLMAT compared to other devices as JUDITH2, it cannot be confirmed that the cracks will grow continuously and so a ductile cracking may be confirmed. In the future, with a new, cooled beam dump at OLMAT, a larger number of pulses (thousands) will be easily achieved which will ease the cracking detection.
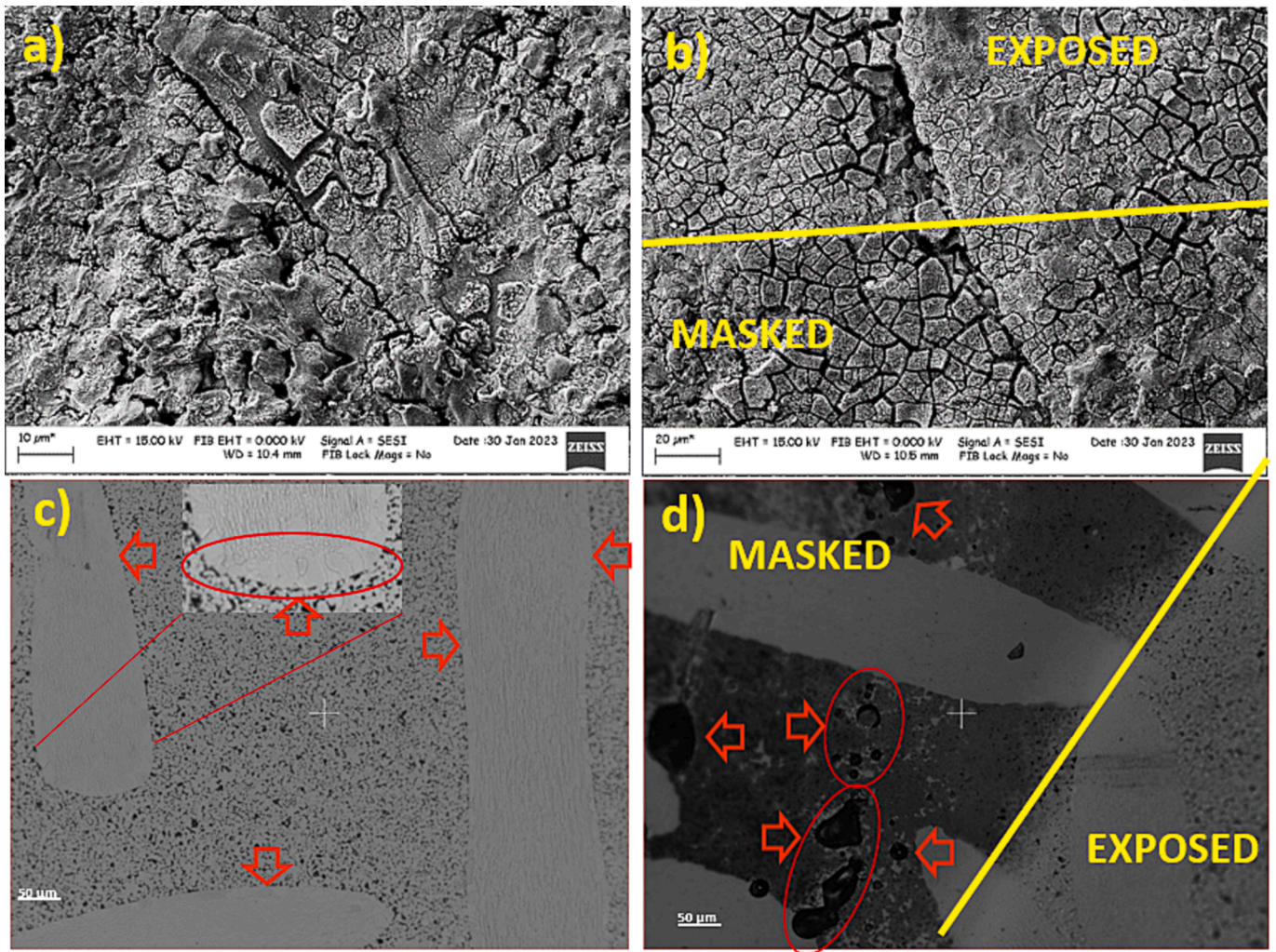
3.2. Porous Matrix PM-Wf/W

During the experiments the temperature reached after a few pulses (~700 °C) should allow the material to be in the ductile regime, and only enter in the fragile regime after the cool down at the technical stops (150–200 °C). This may be true if we consider the usual DBTT of W materials between 250 and 400 °C [4]. However, this kind of material has a pseudo-ductile behavior in the exposed range of temperature due to the fiber and the porous matrix formed by sintered W grains [17,18]. Therefore, only ductile cracking should be considered, as in ITER-like W. Moreover, also as ITER-like W, the maximum temperature reached measured by pirometry has always been under recrystallization temperature: <1200 °C.

As expected, this material showed a much larger resilience against fatigue cracking compared to ITER-like W thanks to its extrinsic toughening mechanisms such as fiber pullout, fiber deformation, crack deflection, and interfacial debonding. Both mirror-polished and as-fabricated Porous Matrix PM-Wf/W samples were exposed in OLMAT to the same heat load where cracking was seen in ITER-like W, but at a larger number of pulses: 950 and 934 pulses (100 ms duration) respectively of 15 ± 5 MW/m² every 45 s for a $F_{HF} = 4.2 \pm 1.4, 4.7 \pm 1.5$ and 5.2 ± 1.6 MW/m²s$^{0.5}$. Although some cracks seem to be present in the exposed part of the as-fabricated Porous Matrix PM-Wf/W, as

shown in Fig. 4a, no surface modification is observed compared to the masked part. Both areas can be compared at Fig. 4b, where even some cracks seem to be present. Both parts have a large quantity of small grains agglomerating into larger grains with clear interfaces. On the mirror-polished samples, no cracks or surface modification were found, as in Fig. 4c. This may indicate that the as-fabricated samples developed no cracks during exposure, as more likely they were fabrication defects at surface that were eliminated with polishing. But small recrystallization was found at the borders of some fibers (red arrows in Fig. 4c). This indicates a local overheating of the fibers at more than 1900 °C, as they are made of K-doped W of high recrystallization temperature [12]. This overheating cannot be detected by pirometry as it measures the whole sample. This has been observed in as-fabricated sampled caused by the sintering process. But as it has been observed only in small areas in the smap,les of this work, this may also be caused by the low thermal conductivity, general and mainly local, of this kind of Wf/W due to the absence of a binder [17,18]. In a future nuclear fusion reactor this local overheating and loss of thermal conductivity could be dangerous so new Wf/W are being developed at Jülich FZ to solve this.

However, the erosion found in both mirror-polished and as-fabricated Porous Matrix PM-Wf/W is quite large compared to the negligible one found with ITER-like W. Mass losses of 25 ± 0.6, 32 ± 0.6 and 33 ± 0.6 mg in mirror-polished samples and 12 ± 0.6, 20 ± 0.6 and 21 ± 0.6 mg in as-fabricated samples were measured at $F_{HF} = 4.2 \pm 1.4$, 4.7 ± 1.5 and 5.2 ± 1.6 MW/m²s$^{0.5}$ respectively. The larger erosion of polished samples has already been ascribed to a larger redeposition of sputtered particles in as-fabricated samples [17]. However, in PSI-2 device the erosion of Porous Matrix PM-Wf/W was even lower than ITER-like W [17]. At SEM no erosion of full loose grains were evident in as-fabricated samples comparing exposed and masked parts as in Fig. 4b, although it is quite difficult to discern due to the extremely rough nature of the sample. However, in the confocal microscope images comparing exposed and masked parts, Fig. 4d, in the masked area some holes of particles that have been lost can be seen, but there are none in exposed areas. The Porous Matrix PM-Wf/W samples had to be machined at the borders to fit into the mask. Perhaps those borders were damaged and some loose particles (due to the grainy nature of Porous Matrix PM-Wf/W) were lost when removing the samples from the TZM mask. This would explain this particle loss and hence the larger mass loss in Porous Matrix PM-Wf/W compared to ITER-like W. However, this explanation is very speculative, so we will improve our procedures to avoid this. In the future, the new mask and W samples design will leave no masked area, and the fit will be easier. Therefore, we hope the erosion will be

Fig. 4. SEM upper images of a as-fabricated Porous Matrix PM-Wf/W sample exposed to 934 pulses of $F_{HF} = 5.2 \pm 1.6$ MW/m^{2}s$^{0.5}$: a) fully exposed surface, b) masked border. Confocal microscope upper images of a mirror-polished Porous Matrix PM-Wf/W sample exposed to 950 pulses of $F_{HF} = 5.2 \pm 1.6$ MW/m^{2}s$^{0.5}$: c) fully exposed surface with red arrows for recrystallization at the border of the fibers with an inset amplifying one fiber edge for a clearer view, d) masked border with holes marked with arrows and within red lines. (For interpretation of the references to colour in this figure legend, the reader is referred to the web version of this article.)

properly measured.

4. Conclusions and future work

OLMAT HHF device has successfully shown its capabilities for thermal fatigue testing of two different types of W armor for ITER and future nuclear fusion reactors: ITER-like W and Porous Matrix PM-Wf/W. As expected, ITER-like W has shown a lower threshold for fatigue damage in agreement with other HHF devices like JUDITH2 in terms of heat flux: $F_{HF} = 5.2 \pm 1.6$ MW/m^{2}s$^{0.5}$. However, the number of pulses necessary for small intergranular cracking to appear is much lower in OLMAT, and it may be related to H embrittlement caused by the high-energy H bombardment in OLMAT (tens keV). In the future, this H embrittlement will be separated from fatigue cracking thanks to the irradiation with the new 90 J CW laser at OLMAT, so both damages types may be separated. This will allow a pure thermal irradiation more similar to JUDITH2. Opposed to this, Porous Matrix PM-Wf/W, specifically designed against cracking damage, as fatigue is, has shown no fatigue damage up to the limit reached here 950 pulses at $F_{HF} = 5.2 \pm 1.6$ MW/m^{2}s$^{0.5}$. In the future, with a new cooled, large sample holder, the current technical issues for the number of pulses per day will be overcome and the targets may be subjected to a larger number of pulses. All these experiments will

help to understand the complex interaction between many parameters (loading conditions, material thermal and mechanical properties, etc) on the thermal shock performance of advanced W armor materials. Moreover, in this way, the comparison to other HHF devices will be easier.

A discrepancy compared to other HHF devices, PSI-2 in this case, has been found for PM-Wf/W samples. The erosion of Porous Matrix PM-Wf/W was lower than ITER-like W in PSI-2 but in OLMAT the mass loss of ITER-like W was negligible, whereas in Porous Matrix PM-Wf/W was very large (12–33 mg). Nevertheless, this larger mass loss is most likely not caused by erosion of exposed parts, but by particle losses at the masked part due to the previous machining of the samples to fit into the mask. This will be solved with a new mask and sample design for a better fit into the mask.

In a future nuclear fusion reactor, like EU-DEMO, fatigue damage will be very relevant, and one of the main design parameters for the advanced W armor materials like Wf/W [1–4,7,8]. Even if the ELM power deposition is reduced to tens of MW/m^2 (e.g. a transient of 2 ms and 0.1 MJ/m^2 energy means a $F_{HF} = 2.2$ MW/m^{2}s$^{0.5}$ not far from the damage threshold) to avoid direct damage by shallow melting, frequencies of tens of Hz will be needed for those ELMs. This means that after just a few days of EU-DEMO operation 10^6 ELMs may be reached (e. g. 20 Hz ELMs means about 14 operation hours), while at ITER, with

much lower duty cycle, this will not be a big issue. It is not clear at all that any advanced W material will be able to withstand such a huge number of fatigue cycles, apart from the technical difficulties to reach those number of cycles in a HHF device [11]. Therefore, at OLMAT new advanced W materials apart from the ones tested here (nanostructured, W alloys…) will be studied to elucidate if ELMy operating modes are a realistic possibility for future nuclear fusion reactors, or ELM-free modes will have to be used in spite of their other disadvantages, like lower confinement and large changes in DEMO design.

CRediT authorship contribution statement

D. Alegre: Writing – original draft, Conceptualization, Data curation, Formal analysis, Investigation. **D. Tafalla:** Investigation, Writing – review & editing. **A. De Castro:** Investigation, Writing – review & editing. **M. González:** Resources. **J.G. Manchón:** Investigation. **F.L. Tabarés:** Supervision, Funding acquisition, Writing – review & editing. **T. Hernández:** Resources. **M. Wirtz:** Methodology, Resources, Writing – review & editing. **J.W. Coenen:** Methodology, Resources, Writing – review & editing. **Y. Mao:** Resources, Writing – review & editing. **E. Oyarzábal:** Supervision, Investigation, Writing – review & editing.

Declaration of competing interest

The authors declare that they have no known competing financial interests or personal relationships that could have appeared to influence the work reported in this paper.

Data availability

Data will be made available on request.

Acknowledgements

References

[1] R.A. Pitts, X. Bonnin, F. Escourbiac, H. Frerichs, J.P. Gunn, T. Hirai, A. S. Kukushkin, E. Kaveeva, M.A. Miller, D. Moulton, V. Rozhansky, I. Senichenkov, E. Sytova, O. Schmitz, P.C. Stangeby, G. De Temmerman, I. Veselova, S. Wiesen, Physics basis for the first ITER tungsten divertor, Nucl. Mater. Energy 20 (2019) 100696, https://doi.org/10.1016/j.nme.2019.100696.

[2] J. Linke, J. Du, T. Loewenhoff, G. Pintsuk, B. Spilker, I. Steudel, M. Wirtz, Challenges for plasma-facing components in nuclear fusion, Matter Radiat. Extremes 4 (2019) 056201, https://doi.org/10.1063/1.5090100.

[3] F. Maviglia, M. Siccinio, C. Bachmann, W. Biel, M. Cavedon, E. Fable, G. Federici, M. Firdaouss, J. Gerardin, V. Hauer, I. Ivanova-Stanik, F. Janky, R. Kembleton, F. Militello, F. Subba, S. Varoutis, C. Vorpahl, Impact of plasma-wall interaction and exhaust on the EU-DEMO design, Nucl. Mater. Energy 26 (2021) 100897, https://doi.org/10.1016/j.nme.2020.100897.

[4] M. Rieth, R. Doerner, A. Hasegawa, Y. Ueda, M. Wirtz, Behavior of tungsten under irradiation and plasma interaction, J. Nucl. Mater. 519 (2019) 334–368, https://doi.org/10.1016/j.jnucmat.2019.03.035.

[5] H. Greuner, B. Böswirth, K. Hunger, A. Khan, T.R. Barrett, F. Gallay, M. Richou, E. Visca, A.V. Müller, J.H. You, Assessment of the high heat flux performance of European DEMO divertor mock-ups, Phys. Scr. 2020 (2020) 014003, https://doi.org/10.1088/1402-4896/ab3681.

[6] H. Greuner, B. Böswirth, T.R. Barrett, F. Crescenzi, F. Gallay, K. Hunger, M. Richou, E. Visca, A. von Müller, J.H. You, Progress in high heat flux testing of European DEMO divertor mock-ups, Fusion Eng. Des. 146 (2019) 216–219, https://doi.org/10.1016/j.fusengdes.2018.12.021.

[7] J.H. You, G. Mazzone, E. Visca, H. Greuner, M. Fursdon, Y. Addab, C. Bachmann, T. Barrett, U. Bonavolontà, B. Böswirth, F.M. Castrovinci, C. Carelli, D. Coccorese, R. Coppola, F. Crescenzi, C. Di Gironimo, P.A. Di Maio, G. Di Mambro, F. Domptail, D. Dongiovanni, G. Dose, D. Flammini, L. Forest, P. Frosi, F. Gallay, B.E. Ghidersa, C. Harrington, K. Hunger, V. Imbriani, M. Li, A. Lukenskas, A. Maffucci, N. Mantel, D. Marzullo, T. Minniti, A.V. Müller, S. Noce, M.T. Porfiri, A. Quartararo, M. Richou, S. Roccella, D. Terentyev, E. Vallone, S. Ventre, R. Villari, F. Villone, C. Vorpahl, K. Zhang, Divertor of the European DEMO: Engineering and technologies for power exhaust, Fusion Eng. Des. 175 (2022) 113010, https://doi.org/10.1016/j.fusengdes.2022.113010.

[8] J.H. You, C. Bachmann, V.G. Belardi, M. Binder, D. Bowden, G. Calabrò, P. Fanelli, M. Fursdon, I.E. Garkusha, S. Gerashchenko, K. Hunger, R. de Luca, V.A. Makhlai, N. Mantel, F. Maviglia, A. v. Müller, N. Nemati, J. Roberts, F. Vivio, Z. Vizvary, K. Zhang, Limiters for DEMO wall protection: Initial design concepts & technology options, Fusion Eng. Des. 174 (2022) 112988. 10.1016/j.fusengdes.2021.112988.

[9] S. Herashchenko, O.V. Byrka, V. Makhlai, M. Wirtz, N.N. Aksenov, I.E. Garkusha, Y. Petrov, S. Malykhin, s. V. Surovitskiy, S. Masuzaki, M. Tokitani, S.I. Lebedev, P. B. Shevchuk, Damaging of pure tungsten with different microstructure under sequential QSPA and LHD plasma loads, Problems Atomic Sci. Technol. (2020) 78–82. 10.46813/2020-130-078.

[10] M. Wirtz, S. Bardin, A. Huber, A. Kreter, J. Linke, T.W. Morgan, G. Pintsuk, M. Reinhart, G. Sergienko, I. Steudel, G.D. Temmerman, B. Unterberg, Impact of combined hydrogen plasma and transient heat loads on the performance of tungsten as plasma facing material, Nucl. Fusion 55 (2015) 123017, https://doi.org/10.1088/0029-5515/55/12/123017.

[11] M. Wirtz, J. Linke, T.h. Loewenhoff, G. Pintsuk, I. Uytdenhouwen, Transient heat load challenges for plasma-facing materials during long-term operation, Nucl. Mater. Energy 12 (2017) 148–155, https://doi.org/10.1016/j.nme.2016.12.024.

[12] P. Lied, W. Pantleon, C. Bonnekoh, S. Bonk, A. Hoffmann, J. Reiser, M. Rieth, Comparison of K-doped and pure cold-rolled tungsten sheets: Tensile properties and brittle-to-ductile transition temperatures, J. Nucl. Mater. 544 (2021) 152664, https://doi.org/10.1016/j.jnucmat.2020.152664.

[13] S. Nogami, G. Pintsuk, K. Matsui, S. Watanabe, M. Wirtz, T. Loewenhoff, A. Hasegawa, Thermal shock behavior of potassium doped and rhenium added tungsten alloys, Phys. Scr. 2020 (2020) 014020, https://doi.org/10.1088/1402-4896/ab3dcc.

[14] E. Sal, C. García-Rosales, K. Schlueter, K. Hunger, M. Gago, M. Wirtz, A. Calvo, I. Andueza, R. Neu, G. Pintsuk, Microstructure, oxidation behaviour and thermal shock resistance of self-passivating W-Cr-Y-Zr alloys, Nucl. Mater. Energy 24 (2020) 100770, https://doi.org/10.1016/j.nme.2020.100770.

[15] A. Calvo, K. Schlueter, E. Tejado, G. Pintsuk, N. Ordás, I. Iturriza, R. Neu, J. Y. Pastor, C. García-Rosales, Self-passivating tungsten alloys of the system W-Cr-Y for high temperature applications, Int. J. Refract Metal Hard Mater. 73 (2018) 29–37, https://doi.org/10.1016/j.ijrmhm.2018.01.018.

[16] A. Terra, G. Sergienko, A. Kreter, Y. Martynova, M. Rasiński, M. Wirtz, T. h. Loewenhoff, G. Pintsuk, D. Dorow-Gerspach, Y. Mao, D. Schwalenberg, L. Raumann, J.W. Coenen, S. Brezinsek, B. Unterberg, C.h. Linsmeier, Micro-structured tungsten, a high heat flux pulse proof material, Nucl. Mater. Energy 25 (2020) 100789, https://doi.org/10.1016/j.nme.2020.100789.

[17] Y. Mao, J.W. Coenen, A. Terra, L. Gao, A. Kreter, M. Wirtz, C. Liu, C. Chen, J. Riesch, Y. Wu, C. Broeckmann, C. Linsmeier, Demonstrating tungsten fiber-reinforced porous-matrix tungsten composites for future fusion application, Nucl. Fusion 62 (2022) 106029, https://doi.org/10.1088/1741-4326/ac8c55.

[18] Y. Mao, J. Coenen, S. Sistla, C. Liu, A. Terra, X. Tan, J. Riesch, T. Hoeschen, Y. Wu, C. Broeckmann, C. Linsmeier, Design of tungsten fiber-reinforced tungsten composites with porous matrix, Mater. Sci. Eng. A 817 (2021) 141361, https://doi.org/10.1016/j.msea.2021.141361.

[19] J.W. Coenen, Y. Mao, S. Sistla, A. v. Müller, G. Pintsuk, M. Wirtz, J. Riesch, T. Hoeschen, A. Terra, J.-H. You, H. Greuner, A. Kreter, Ch. Broeckmann, R. Neu, Ch. Linsmeier, Materials development for new high heat-flux component mock-ups for

DEMO, Fusion Eng. Des. 146 (2019) 1431–1436. 10.1016/j. fusengdes.2019.02.098.

[20] D. Alegre, E. Oyarzabal, D. Tafalla, M. Liniers, A. Soleto, F.L. Tabarés, Design and Testing of Advanced Liquid Metal Targets for DEMO Divertor: The OLMAT Project, J Fusion Energ 39 (2020) 411–420, https://doi.org/10.1007/s10894-020-00254-5.

[21] F.L. Tabarés, E. Oyarzabal, D. Alegre, D. Tafalla, K.J. McCarthy, A. de Castro, E. Ascasíbar, A. Soleto, I. Fernández-Berceruelo, R. Carrasco, F. Martin, J. A. Sebastián, J. Gómez-Manchón, A. Pereira, A. de la Peña, Commissioning and first results of the OLMAT facility, Fusion Eng. Des. 187 (2023) 113373, https://doi.org/10.1016/j.fusengdes.2022.113373.

[22] A. de Castro, E. Oyarzábal, D. Alegre, D. Tafalla, M. González, K.J. McCarthy, J.G. A. Scholte, T.W. Morgan, F.L. Tabarés, the OLMAT team, Physics and Technology Research for Liquid-Metal Divertor Development, Focused on a Tin-Capillary Porous System Solution, at the OLMAT High Heat-Flux Facility, J. Fusion Energ 42 (2023) 45, https://doi.org/10.1007/s10894-023-00373-9.

[23] E. Oyarzabal, F.L. Tabarés, M. Liniers, D. Alegre, D. Tafalla, K.J. McCarthy, A. de Castro, T.W. Morgan, J.G.A. Scholte, M. Iafrati, E. de la Cal, I. Voldimer, E. Ascasíbar, A. Soleto, Comparative study of different Sn wetted W CPSs exposed to NBI fluxes in the OLMAT facility, Fusion Eng. Des. 190 (2023) 113711, https://doi.org/10.1016/j.fusengdes.2023.113711.

[24] M. Liniers, J. Damba, J. Guasp, J.A. Sebastián, F. Martín, B. Rojo, R. Carrasco, E. Sánchez, F. Miguel, G. Wolfers, A. Soleto, E. Ascasíbar, Beam transmission dependence on beam parameters for TJ-II Neutral Beam Injectors, Fusion Eng. Des. 123 (2017) 259–262, https://doi.org/10.1016/j.fusengdes.2017.05.104.

[25] M. Gago, A. Kreter, B. Unterberg, M. Wirtz, Synergistic and separate effects of plasma and transient heat loads on the microstructure and physical properties of ITER-grade tungsten, Phys. Scr. 96 (2021) 124052, https://doi.org/10.1088/1402-4896/ac326c.

[26] M. Gago, A. Kreter, B. Unterberg, M. Wirtz, Synergistic effects of particle and transient heat loads on ITER-grade tungsten, Phys. Scr. 2020 (2020) 014007, https://doi.org/10.1088/1402-4896/ab3bd9.